

Viewing the early stage of foam formation by high-resolution computed tomography

L. Helfen, T. Baumbach

Fraunhofer IZFP, Saarbrücken / Dresden, Germany

H. Stanzick, J. Banhart

Fraunhofer IFAM, Bremen, Germany

A. Elmoutaouakkil, P. Cloetens

European Synchrotron Radiation Facility, Grenoble, France

K. Schladitz

Fraunhofer ITWM, Kaiserslautern, Germany

Aluminium AlSi7 alloy (7 wt-% of Si) foam is investigated by μm -resolved x-ray computed tomography (CT) using synchrotron radiation. The foam is fabricated employing a powder metallurgical route. The evolution of the foam microstructure in a series of samples representing different stages of foam expansion is studied. The series is obtained by interrupting the foaming process for each sample at different foaming time. The 3D computer tomographic reconstruction provides the 3D pore structure as well as the distribution of foaming agent particles. Statistical evaluation allows to determine the size distribution of the foaming agent and the pores at different foaming stages.

1 Introduction

Although the technology for producing metallic foams is rather well controlled the principle physics underlying the foaming process are not yet fully understood. Some aspects of metallic foams such as the stabilising mechanisms for the liquid foam [1] or the pore nucleation process are still rather poorly explored. Until now, laboratory CT using x-ray tubes has been used for 3D imaging of metallic foams [2] but they usually lack the resolution and quality for viewing the features occurring at the early stage of foam formation.

In this paper we report results obtained by synchrotron microtomography which give evidence on the pore nucleation process and early foaming stages of AlSi7 foams.

2 Sample preparation

A series of aluminium alloy samples has been fabricated employing a powder metallurgical method [3]. This procedure is based on the mixing of two or more powders, usually the

alloy powder and a gas releasing blowing (foaming) agent. Here, three powders have been used, namely powders of pure aluminium and silicon to form an AlSi7 alloy (7 wt-% of Si) with the addition of 0.6 wt-% of a TiH_2 powder as the blowing agent. Subsequently, this blend was compacted to a foamable precursor material by conventional axial (closed-die) compaction at a temperature of 450 °C and a pressure of 120 MPa. The resulting tablets were virtually dense (≤ 0.75 % porosity).

The foaming process was triggered by heating the precursor material within a pre-heated furnace set to a temperature of 600 °C. During the heating process the blowing agent starts to release the blowing gas hydrogen at temperatures of 380...400 °C and fissure-like pores form in the material. Far before the foam had reached its maximum expansion, the foaming process was interrupted by quenching the sample in cold air, freezing the porous structure. Different porosities $\varepsilon = 0.24, 0.28, 0.32$ and 0.43 in the sample series were obtained for corresponding foaming times (including the heating) of 200 s, 240 s, 300 s and 420 s, respectively. Of the partly foamed materials, volumes of $5 \times 5 \times 30 \text{ mm}^3$ have been cut out by spark erosion from which a region of almost $5 \times 5 \times 7 \text{ mm}^3$ has been investigated by CT.

3 Experimental method

On each of the pre-foamed samples, tomographic scans have been carried out in order to determine their microstructure [4]. The x rays are attenuated along their path through the sample according to the integral of its attenuation coefficient along this path. Taking different x-ray radiographs for various sample rotation angles allows to calculate its 3D attenuation distribution.

Experiments have been performed at the imaging facilities of beamline ID19 at the ESRF, see, e. g. [5]. In contrast to conventional CT using x-ray tubes providing a conic beam, we use the nearly parallel synchrotron beam, which can be monochromatised easily by Bragg diffraction (double crystal monochromator, employing the 111-reflection of perfect silicon crystals). Using monochromatic radiation permits to reconstruct quantitatively the linear attenuation coefficient μ for the selected energy (see Table 1) and avoids artefacts in the reconstructed image. The attenuation coefficient is directly related to the atomic number and the density of the material.

The samples filled out almost the entire field of view of the electronic detector system, a scintillator crystal coupled by visible-light optics to a CCD. Pixel size was $6.7 \mu\text{m}$ on a 1024×1024 pixels CCD, resulting in a field of view of almost 7 mm. The x-ray energy was chosen individually for every sample allowing to optimise the contrast in the radiographic projections. Taking 900 projection radiographs for each sample, the volume structure has been reconstructed into 3D images of the linear attenuation coefficient μ .

4 Results

Fig. 1 shows for each sample one representative 2D slice within a plane parallel to the axis of powder compaction taken from the reconstructed 3D images. The gray level values within the images correspond to the reconstructed linear attenuation coefficient μ . With increasing porosity ε the pores (black zones) occupy larger fractions of volume and develop in a typical way from thin fissures to rather spherical bubbles. The blowing agent and

highly absorbing impurities are almost spherical and visible as the light spots. For the larger porosities ($\varepsilon = 0.32, 0.43$) the population of the blowing agent located at the pore walls appears to increase. The rest of the gray values in Fig. 1 correspond to the AlSi7 matrix. In Table 1 the porosity and the mean reconstructed absorption coefficients of the alloy at the chosen x-ray energies are given.

Various digital image processing techniques have been employed in order to isolate every pore and blowing agent particle within the 3D image of μ and to determine their respective sizes and positions. From this data we have determined *statistical* properties of

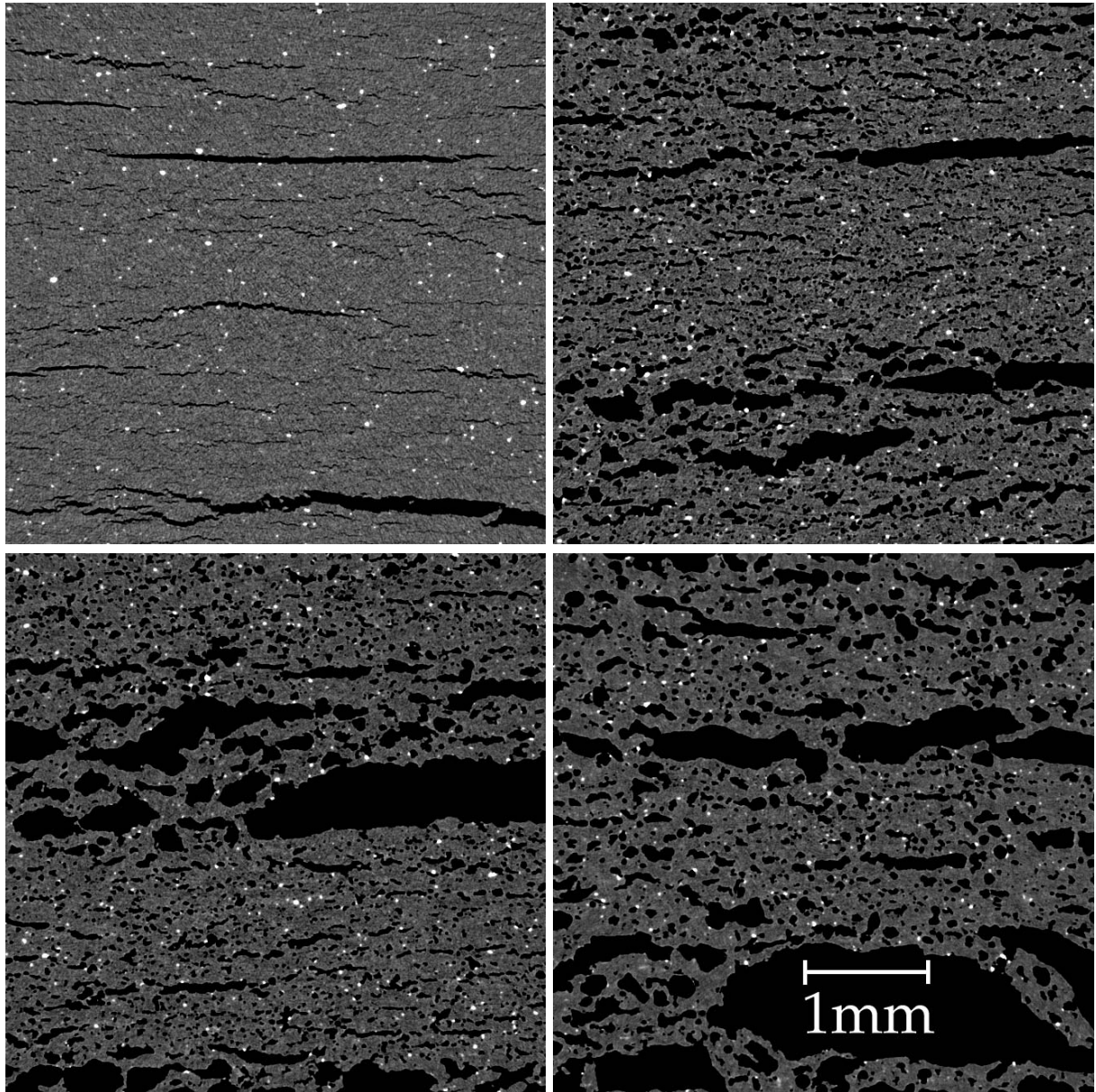


Figure 1: Reconstructed slices of the AlSi7 samples: $\varepsilon = 0.24, 0.28, 0.32, 0.43$ (from top left to bottom right). Image sizes are 660×660 with a pixel size of $6.7 \mu\text{m}$. The samples were compacted along an axis parallel to the top-down orientation in the image. The light spots are regions with a large linear attenuation coefficient μ , corresponding to the strongly absorbing blowing agent and residual impurities.

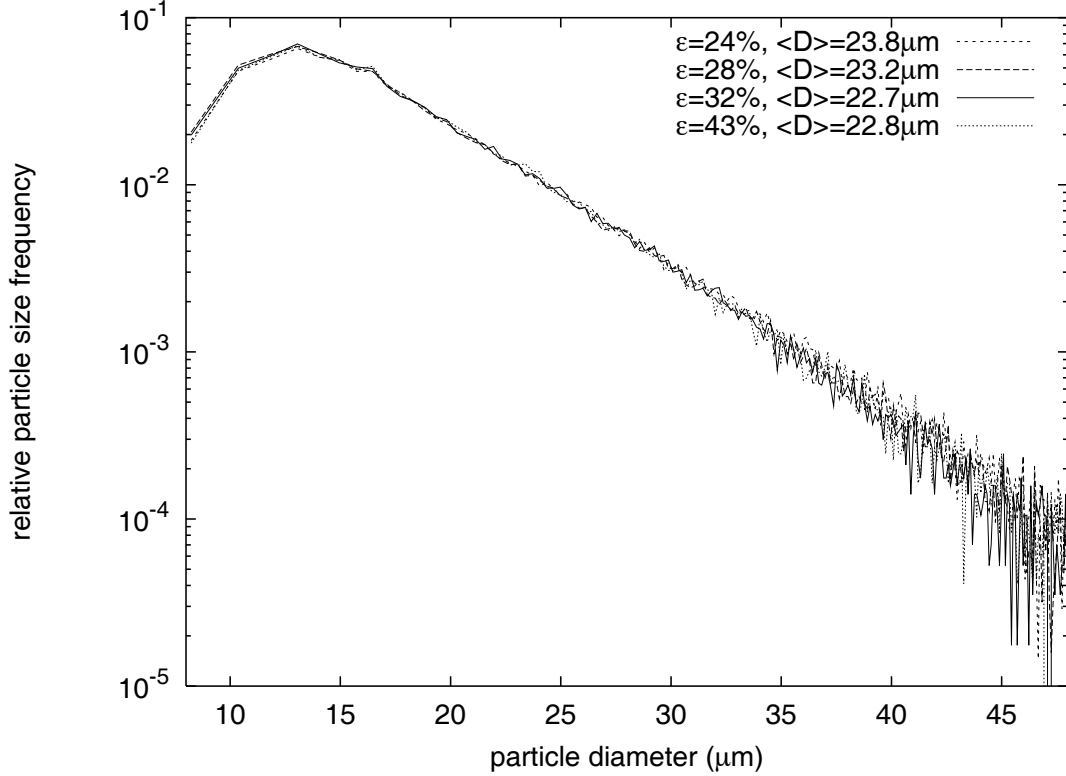


Figure 2: Diameter distribution of the blowing agent particles of the investigated samples in a semi-logarithmic plot. $\langle D \rangle$ indicates the mean diameter of the particles.

the foam evolution in terms of volume fractions, mean sizes, total numbers and size distribution functions of the blowing agent particles and the pores, respectively. The results are summarised in Figs. 2–4 and Table 1. Note that the porosities ε measured macroscopically on the entire samples agree well with the pore volume fractions determined by 3D image processing on the imaged region except for $\varepsilon = 0.24$.

As the blowing agent particles are almost spherical we express, therefore, their size distribution in terms of particle diameter rather than volume. The blowing agent particle size distribution for the studied sample volumes is plotted in Fig. 2, normalized to the total particle number. For all samples the particle size distribution behaves similarly, indicating that the foaming process does not alter significantly the size of the blowing agent particles. The most frequent size is around $14 \mu\text{m}$ with a mean size at around $23 \mu\text{m}$ for all samples, agreeing with results of laser particle analysis performed on the base powders.

The pores are strongly oblate with their short extension parallel to the compaction axis. The temporal evolution of their size distribution in terms of pore volume is shown in Fig. 3, and in Fig. 4 normalized with respect to the total pore number. From Fig. 3 and Table 1 we find first an increase of the total pore number (by a factor of 4 from $\varepsilon = 0.24$ to $\varepsilon = 0.28$), and afterwards a reduction of the total pore number ($\varepsilon = 0.32$ and $\varepsilon = 0.43$). Hence, the number of pores per unit volume N_{tot}/V decreases for the latter stages investigated which may be emphasised by the presence of a few huge pores occupying large a fraction of space within the 3D image. Fig. 4 describes quantitatively how the relative number of medium- and large-sized pores increases with foam expansion,

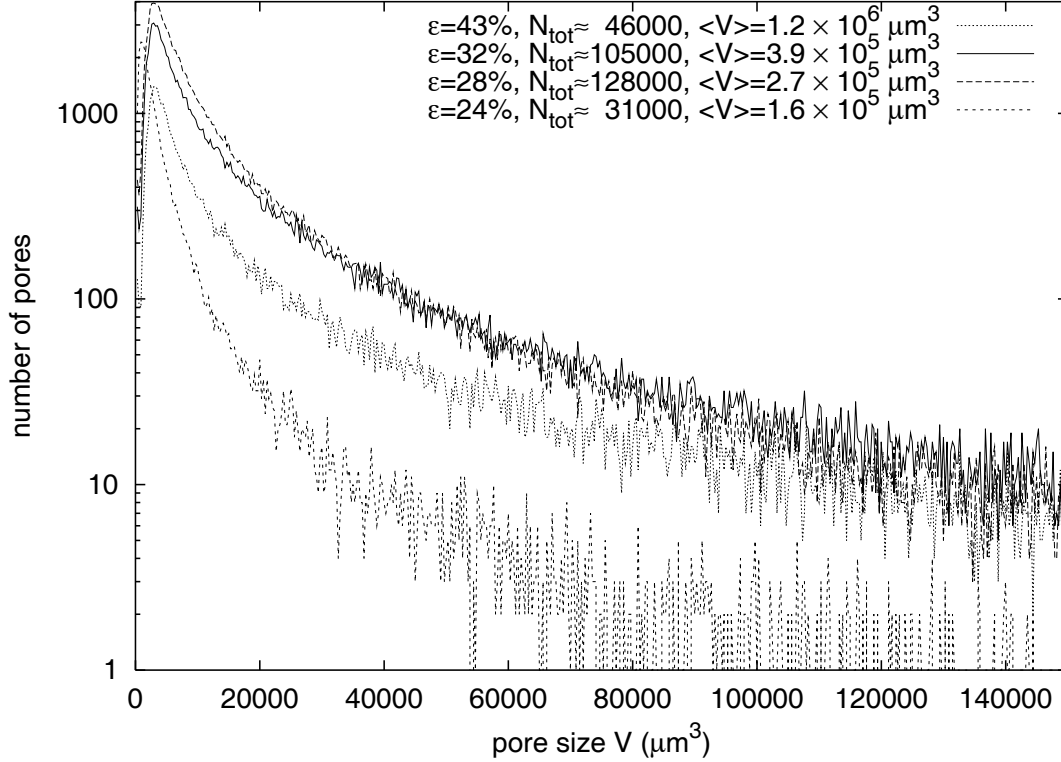


Figure 3: Absolute volume distribution of the pores of the investigated samples in a semi-logarithmic plot. N_{tot} denotes the total number of pores, $\langle V \rangle$ their mean size.

Sample porosity ε	foaming time in s	x-ray energy E in keV	reconstr. $\langle \mu_{\text{AlSi7}} \rangle$ in cm^{-1}	pores volume fraction	mean size in μm^3	b. agent volume fraction	mean diameter in μm
0.24	200	30	2.67	0.038	1.6×10^5	0.0036	23.3
0.28	240	30	2.79	0.261	2.7×10^5	0.0043	23.2
0.32	300	27	3.69	0.308	3.9×10^5	0.0040	22.7
0.43	420	25	4.56	0.410	1.2×10^6	0.0040	22.8

Table 1: Sample preparation, experimental parameters and results for the sample series. The stated porosity was measured by determining the mass and volume of the whole sample ($5 \times 5 \times 30 \text{ mm}^3$) whereas the stated volume fractions are obtained along with the mean sizes by 3D image analysis. The volume fraction corresponding to 0.6 wt-% of TiH_2 would be 0.0042.

hence with proceeding foaming time. The increase of porosity is therefore mainly due to pore growth rather than new pore nucleation.

5 Conclusions

Synchrotron CT is a well adapted method for viewing the early foaming stages and pore nucleation in metallic foams. Pores and blowing agent particles have been investigated

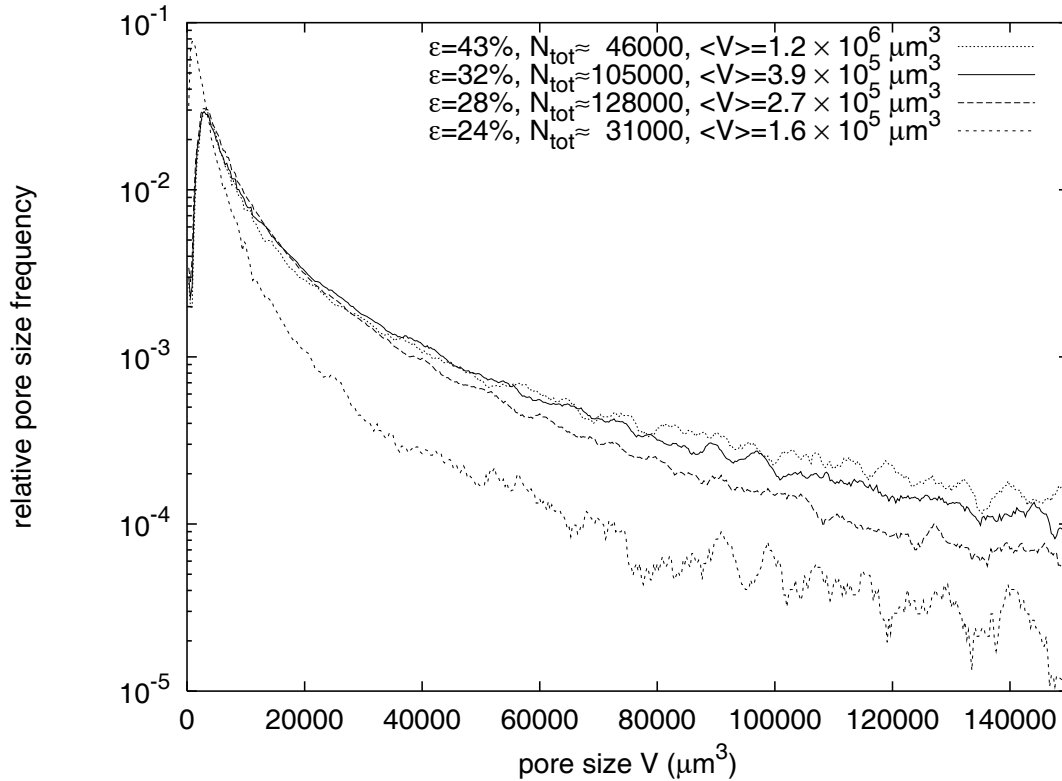


Figure 4: Relative volume distribution of the pores of the sample series with smoothed data in a semi-logarithmic plot. N_{tot} denotes the total number of detected pores. Note that their mean size $\langle V \rangle$ lies outside the plotted pore size range, confirming that huge pores occupy a significant amount of volume.

non-destructively, allowing us to circumvent problems encountered during sample preparation, e. g. deterioration introduced by cut edges or polishing. 3D image analysis gives size distributions of pores and blowing agent particles. This allows to draw conclusions about the inhomogeneity of the foam structure, giving valuable hints about the perfection of the fabrication process and helping improving it. Further evaluation of the 3D data will allow us to determine the relative positions of the blowing agent particle with respect to the pores in order to clarify the pore nucleation process.

References

- [1] J. Banhart, H. Stanzick, L. Helfen, T. Baumbach, *Appl. Phys. Lett.* **78**, 1152 (2001)
- [2] J. Baruchel, J.-Y. Buffière, E. Maire, P. Merle, G. Peix, “X-ray Tomography in Materials Science”, *Hermes Science Publications* (2000)
- [3] J. Banhart, *europysics news* **30**, 17 (1999)
- [4] L. Helfen, H. Stanzick, J. Banhart, T. Baumbach, *ESRF Highlights 2001*, 84 (2001)
- [5] M. Salomé, F. Peyrin, P. Cloetens, C. Odet, A.-M. Laval-Jeantet, J. Baruchel, P. Spanne, *Med. Phys.* **26**, 2194 (1999)